BIOCHEMISTRY
including biophysical chemistry & molecular biology
Article

Biochemistry **2010,** *49,* 9361–9371 9361
DOI: 10.1021/bi100833r

Long-Range Interaction Networks in the Function and Fidelity of Poliovirus RNA-Dependent RNA Polymerase Studied by Nuclear Magnetic Resonance†

Xiaorong Yang,‡,∥ Jesse L. Welch,‡,∥ Jamie J. Arnold,§ and David D. Boehr*,‡

‡*Department of Chemistry and* §*Department of Biochemistry and Molecular Biology, The Pennsylvania State University, University Park, Pennsylvania 16802, United States* ∥*These authors contributed equally to this work*

Received May 25, 2010; Revised Manuscript Received September 6, 2010

ABSTRACT: The fidelity of the poliovirus RNA-dependent RNA polymerase ($3D^{pol}$) plays a direct role in the genomic evolution and pathogenesis of the virus. A single site mutation (Gly64Ser) that is remote from the catalytic center results in a higher fidelity polymerase. NMR studies with [*methyl*-^{13}C]methionine-labeled protein were used to compare the solution structure and dynamics of wild-type and Gly64Ser $3D^{pol}$. The chemical shifts for the Met6 resonance were significantly different between wild-type and Gly64Ser $3D^{pol}$ when bound in ternary complexes with RNA and incorrect, but not with correct, nucleotide, suggesting that the Gly64Ser mutation induces structural changes in the N-terminal β-strand when the enzyme is bound to incorrect but not correct nucleotide. We also observe changes in the transverse relaxation times for methionines near regions important for nucleotide and RNA binding and catalysis. Our strategy to assign the [*methyl*-^{13}C]methionine resonances involved separately mutating each of the 17 methionines. Several substitutions produced additional resonances for both Met6 and Met187, a reporter for RNA binding, and conformational changes in the highly conserved motif B loop, even though these methionines are greater than 20 Å apart. The results for Gly64Ser and the other mutants are intriguing considering that they can result in structural and/or dynamic changes to methionines distant from the site of mutation. We propose that there is a long-distance network operating throughout $3D^{pol}$ that coordinates ligand binding, conformational changes, and catalysis. Mutation of Gly64 results in structural and/or dynamic changes to the network that may affect polymerase fidelity.

Positive-strand RNA[1] viruses cause a variety of acute and chronic diseases in humans including the common cold, myocarditis, hepatitis, severe acute respiratory syndrome (SARS), and liver cancer (*1*−*4*). The enzyme responsible for replicating the genomes of RNA-based viruses is the virally encoded RNA-dependent RNA polymerase ($3D^{pol}$). The polymerase from poliovirus (PV) has emerged as an important model system for understanding the function of $3D^{pol}$ enzymes (*5*). Intriguingly, the error frequency or "fidelity" of PV $3D^{pol}$ appears to be very important to the biology and pathogenesis of poliovirus. For example, restriction of genetic variability within a population of poliovirus through expression of a mutant high-fidelity $3D^{pol}$ leads to lower tissue adaptability and viral pathogenicity (*6*−*9*). This suggests that understanding the function and fidelity mechanisms of $3D^{pol}$ has a direct bearing on disease intervention. Antiviral strategies may include targeting $3D^{pol}$ by small molecules to inhibit its activity and/or change its fidelity (*10*−*13*), or alternatively, virus encoding $3D^{pol}$ enzymes with altered fidelity may be potentially used as live, attenuated vaccine strains (*7*, *14*).

PV $3D^{pol}$ has a "cupped right-hand" structure with fingers, palm, and thumb subdomains that is common to many other RNA and DNA polymerases (*15*−*17*) (Figure 1). Most of the catalytic machinery is found in the palm region, including the conserved structural motifs A−E (*5*, *18*). Asp233 in motif A and Asp328 in motif C help to coordinate magnesium and bind the phosphate groups of the incoming nucleotide (*19*, *20*). The other highly conserved aspartate in motif A, Asp238, along with Asn297 from motif B participates in hydrogen bond interactions with the ribose group of the incoming nucleotide; these interactions are critical for proper sugar selection (*19*−*21*).

There are five proposed kinetic intermediates in the catalytic cycle of $3D^{pol}$: enzyme binds RNA ($E:R_n$), followed by binding of nucleotide to form a ternary complex ($E:R_nNTP$) that then undergoes a conformational change to form a complex competent for phosphoryl transfer ($*E:R_nNTP$). Phosphodiester formation occurs to yield the ternary product complex ($*E:R_{n+1}PP_i$) that then undergoes another conformational change ($E:R_{n+1}PP_i$), followed by the release of pyrophosphate ($E:R_{n+1}$) (*22*, *23*). In PV $3D^{pol}$, the conformational change step prior to phosphoryl transfer and the phosphoryl transfer step itself are both partially rate limiting (*22*, *23*). Thus, correct and incorrect nucleotide incorporation can be distinguished by kinetic differences in both of these steps.

†This work was supported by a Pennsylvania State start-up fund to D. D.B. and NIH Grant AI45818 to J.J.A. and Craig E. Cameron.

*To whom correspondence should be addressed. Tel: 814-863-8605. Fax: 814-863-0618. E-mail: ddb12@psu.edu.

[1]Abbreviations: NMR, nuclear magnetic resonance; HSQC, heteronuclear single-quantum coherence; NOE, nuclear Overhauser effect; TROSY, transverse relaxation optimized spectroscopy; RNA, ribonucleic acid; DNA, deoxyribonucleic acid; $3D^{pol}$, RNA-dependent RNA polymerase; PV, poliovirus; NTP, nucleoside triphosphate; FMDV, foot and mouth disease virus; rmsd, root-mean-square deviation; WT, wild type; PMSF, phenylmethanesulfonyl fluoride; SUMO, small ubiquitin-like modifying protein; UTP, uracil triphosphate; 3′-dATP, 3′-deoxyadenine triphosphate; TEMED, tetramethylethylenediamine; EDTA, ethylenediaminetetraacetic acid; DSS, 4,4-dimethyl-4-silapentane-1-sulfonic acid.

Published on Web 09/23/2010

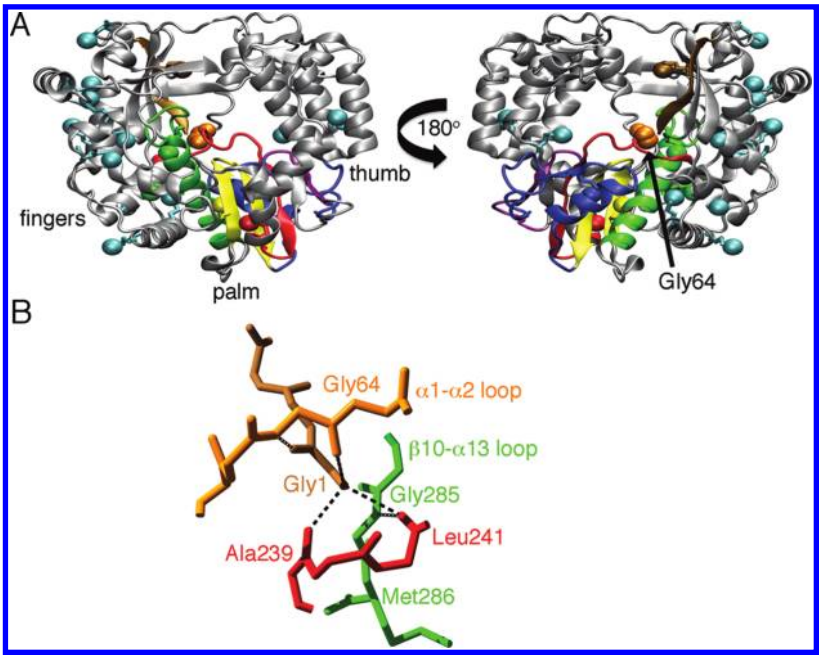

FIGURE 1: Structure of PV 3D^{pol} (PDB 1RA6). (A) The locations of the terminal methyl groups of the methionines are indicated as colored spheres. The conserved structural motifs in the palm subdomain are colored as follows: motif A, red; motif B, green; motif C, yellow; motif D, blue; motif E, purple. Gly64 is colored orange, and the N-terminal β-strand is colored brown. (B) Hydrogen bond interactions involving Gly64, Gly1 on the N-terminal β-strand, Ala239 and Leu241 on motif A, and Gly285 on the β10−α13 loop. Motifs are colored as in (A). Hydrogen bonds are indicated as black lines.

The conformational change prior to chemistry is observed in most replicative nucleic acid polymerases (*16*, *24*). However, there is some controversy concerning the nature of the conformational change (*16*, *25*). It has been suggested that in some nucleic acid polymerases the conformational change is a global "open−closed" conformational change (*16*), but in 3D^{pol} the conformational change step is likely to be more localized and traced to structural changes of motifs A and B (*22*, *23*). For instance, the interaction between Asp238 and Asn297 observed in the unliganded enzyme occludes the ribose-binding pocket, and consequently, there must be a conformational change involving residues in motifs A and B in order for nucleotide to bind (*19*). Further structural changes involving Asp238, Asn297, and other residues in motif B such as Ser288 and Thr293 are also predicted to occur in order for the triphosphate group to align for catalysis (*19*, *22*, *23*). This suggestion is in agreement with crystal structures of foot-and-mouth disease virus (FMDV) 3D^{pol} that show localized structural changes to motifs A and B upon formation of the ternary complex with RNA and nucleoside triphosphate (NTP) (*26*). The highly conserved loop in motif B in FMDV 3D^{pol} (β10−α13 loop according to PV numbering and containing residues 285−293, β9−α11 loop according to FMDV) changes conformation to accommodate different nucleotides and RNA (*26*). The conformational change may also involve structural rearrangements in motif D to bring Lys359 into a position where it can act as a general acid to protonate the pyrophosphate leaving group (*27*, *28*).

Some insight into the function and fidelity of PV 3D^{pol} can be gained by the functional and structural characterization of mutant enzymes that either increase or decrease polymerase fidelity. For example, mutation of the highly conserved Gly64 present on the α1−α2 loop (containing residues 61−71) in the fingers domain to Ser results in a higher fidelity polymerase. The rate of correct nucleotide incorporation is ~6000-fold greater than incorrect nucleotide incorporation for wild-type 3D^{pol}, whereas for Gly64Ser 3D^{pol}, correct nucleotide incorporation is ~9000-fold greater than incorrect nucleotide incorporation (i.e., the fidelity of Gly64Ser 3D^{pol} is ~1.5-fold greater than wild-type 3D^{pol}) (*6*). Thus, for Gly64Ser 3D^{pol}, nucleotide incorporation is more stringent, and this leads to a lower error rate and decreased diversity within the viral population (*6*, *7*). The differences in fidelity are not due to differences in nucleotide binding or to the rates of phosphodiester formation but rather appear to be due to alterations in the conformational change step that brings the enzyme into an active conformation (*6*).

Gly64 is involved in a hydrogen-bonding network that includes residues in the N-terminal β-strand, motif A, and the β10−α13 loop in motif B (Figure 1B). This suggests that mutation of Gly64 to Ser may result in structural changes to the N-terminal β-strand, motif A, and/or the β10−α13 loop. However, comparison of the X-ray crystal structure of the unliganded forms of wild-type (WT) and Gly64Ser 3D^{pol} did not show any significant structural differences in these regions (*29*). The crystal structures of WT and Gly64Ser 3D^{pol} overlapped to a great extent (rmsd = 0.28 Å for the protein backbone), and there were no obvious structural differences that pointed toward changes in function and/or fidelity (*29*, *30*). These results prompted the suggestion that the functional differences may arise not because of structural changes but due to differences in the internal protein motions between WT and Gly64Ser 3D^{pol} (*29*, *30*). However, it should be noted that structural differences might only become apparent when the enzymes are bound to RNA and/or form ternary complexes competent for phosphodiester formation. Unfortunately, there are currently no available structures of WT or Gly64Ser PV 3D^{pol} bound with RNA that would shed more insight.

We have used solution NMR to gain insight into the structural changes that occur when PV 3D^{pol} binds RNA and nucleotide and to identify structural and/or dynamic differences between WT and Gly64Ser 3D^{pol} that might help to explain their

differences in function and fidelity. $3D^{pol}$ is challenging to study by solution NMR, considering that the protein is relatively large by NMR standards (52 kDa). However, there are now a number of established strategies to study larger proteins by NMR (*31*, *32*), including TROSY (transverse relaxation optimized spectroscopy) based methods to study both backbone amide groups and side-chain methyl groups (*33*). In our case, we have isotopically labeled the terminal methyl groups of the methionine residues in the protein. This allowed us to quickly adapt existing protein expression and purification procedures for isotope labeling (*34*). During our studies, we identified a complex, long-distance interaction network operating throughout $3D^{pol}$ that might be responsible for coordinating nucleotide and nucleic acid binding and catalysis. Moreover, the Gly64Ser mutation results in structural and/or dynamic changes to residues on this network. Further delineation of this amino acid network will bring new insights into the fidelity and function of PV $3D^{pol}$ and related polymerases and can be used as leverage in rational viral vaccine and/or inhibitor design.

EXPERIMENTAL PROCEDURES

Site-Directed Mutagenesis. Site-directed mutagenesis was carried out using the QuikChange site-directed mutagenesis kit (Stratagene). Forward and reverse primers were designed for each of the Met site mutations (Supporting Information Table S1). Mutations were confirmed by DNA sequencing (Nucleic Acid Facility, The Pennsylvania State University).

Expression of $3D^{pol}$. Expression and purification of WT and mutant $3D^{pol}$ enzymes followed previous procedures (*34*−*36*) with some minor modifications. For the production of [*methyl*-^{13}C]methionine-labeled $3D^{pol}$, plasmids expressing $3D^{pol}$ were transformed into Met-auxotroph *Escherichia coli* B834(DE3) cells and grown in autoinducible minimal medium containing [ε-$^{13}CH_3$]methionine as described in ref *37*. $3D^{pol}$ is expressed as a fusion protein to SUMO and an N-terminal polyhistidine tag that increases protein production, eases purification, and allows for production of $3D^{pol}$ with the naturally occurring Gly1 (*34*, *36*).

Protein Purification. Buffer B (100 mM potassium phosphate, pH 8.0, 500 mM NaCl, 5 mM imidazole, 5 mM β-mercaptoethanol, 60 μM $ZnCl_2$, and 20% (w/v) glycerol) and buffer C (100 mM potassium phosphate, pH 8.0, 500 mM NaCl, 60 μM $ZnCl_2$, 5 mM β-mercaptoethanol, and 20% (w/v) glycerol) were prepared. Cell pellets were resuspended in 50 mL of lysis buffer (50 mL of buffer B, 1.4 μg/mL pepstatin A, 1 μg/mL leupeptin, 1 mM PMSF, and 0.1% N-P40) and subjected to sonication. Cell lysates were centrifuged at 30000*g* and 4 °C for 30 min. Supernatant was applied to Ni-NTA (Invitrogen) columns preequilibrated with buffer C1 (buffer C, 5 mM imidazole, and 0.1% N-P40). The resin was washed with 3 bed volumes each of buffer C1 and buffer C2 (buffer C, 5 mM imidazole), and protein was eluted using high imidazole buffers C3 (buffer C, 50 mM imidazole) and C4 (buffer C, 500 mM imidazole). The polyhistidine tag and SUMO protein domain were cleaved from $3D^{pol}$ using the protease Ulp1. Protein solutions were dialyzed against 80 mM Tris-HCl, pH 8.0, 500 mM NaCl, 20% (w/v) glycerol, 10 mM β-mercaptoethanol, and 60 μM $ZnCl_2$ overnight (optimal buffer for protease cleavage) and then dialyzed against 100 mM potassium phosphate, pH 8.0, 20% (w/v) glycerol, 10 mM β-mercaptoethanol, and 60 μM $ZnCl_2$ for 2−3 h. A second Ni-NTA column was used to separate the purified $3D^{pol}$ from the cleaved polyhistidine tag/SUMO domain, using procedures identical to the first Ni-NTA column. For WT and Gly64Ser $3D^{pol}$, additional phospocellulose and Q-Sepahrose columns were used to ensure protein solutions were free of trace contaminants of nuclease and phosphatase activities (*34*−*36*). Proteins were >95% homogeneous as estimated by Coomassie blue staining of SDS−PAGE gels. Protein is stable at 4 °C for 3−4 months under high salt conditions (80 mM Tris-HCl, pH 8.0, 500 mM NaCl, 20% (w/v) glycerol, 10 mM β-mercaptoethanol, and 60 μM $ZnCl_2$).

Preparation of RNA Oligonucleotides. The 10-mer single-stranded RNA oligonucleotides (5′-GCAUGGGCCC-3′) were purchased from Dharmacon RNAi Technologies and deprotected before use. Deprotection was performed by resuspending the RNA into 100 mM acetic acid adjusted to pH 3.8 with tetramethylethylenediamine (TEMED) and incubating for 30 min at 60 °C. The RNA solutions were dried by SpeedVac, and the deprotected RNA pellets were then resuspended in ^2H_2O. The final stock concentration of ∼7 mM was determined via the absorbance of the RNA at 260 nm using a calculated extinction coefficient of 90000 M^{-1} cm^{-1}. Importantly, the RNA oligonucleotide was previously designed such that it forms a six base pair duplex flanked by two four-nucleotide 5′ overhangs (*38*). This symmetrical primer/template substrate (sym/sub) RNA has been used extensively in the kinetic analysis of PV $3D^{pol}$ (*22*, *23*).

Activity Assay of $3D^{pol}$−RNA Complex Formation. To ensure we could achieve complex formation with our purified protein ([*methyl*-^{13}C]methionine-labeled WT and Gly64Ser $3D^{pol}$) and the RNA substrate using NMR buffer (10 mM HEPES, pH 8.0, 200 mM NaCl, 5 mM $MgCl_2$, 20 μM $ZnCl_2$, 0.02% NaN_3) in ^2H_2O, reactions were carried out with 500 μM ATP or 3′-dATP and 10 μM ^{32}P-labeled RNA. For comparison, reactions were also performed in H_2O containing 50 mM HEPES, pH 7.5, 10 mM 2-mercaptoethanol, 5 mM $MgCl_2$, 20 μM $ZnCl_2$, 500 μM ATP or 3′-dATP, and 10 μM RNA and without ^{13}C-labeled protein. Reactions were initiated by the addition of $3D^{pol}$ to a final concentration of 1 μM and incubated at 30 °C for 10 min. $3D^{pol}$ was diluted immediately prior to use in 50 mM HEPES, pH 7.5, 10 mM β-mercaptoethanol, 60 μM $ZnCl_2$, and 20% glycerol. Reaction volumes were 50 μL. Reactions were quenched by the addition of ethylenediaminetetraacetic acid (EDTA) to a final concentration of 100 mM. Products were resolved from substrate by electrophoresis through a denaturing polyacrylamide gel, visualized by phosphorimaging, and quantified by using the ImageQuant software (Molecular Dynamics) (see Supporting Information Figure S1).

NMR Sample Preparation. For NMR studies, proteins were concentrated (∼200−400 μM $3D^{pol}$) and then desalted using spin columns (Thermo Scientific) to exchange into NMR buffer. For our initial studies with WT and methionine mutant apoenzymes, and with our $CoCl_2$ titrations and NMR relaxation experiments, protein was exchanged into 25 mM potassium phosphate, pH 8.0, 150 mM NaCl, 1 mM DTT, and 0.02% (w/v) NaN_3 in ^2H_2O. For the RNA and nucleotide binding studies, the buffer used was 10 mM HEPES, pH 8.0, 200 mM NaCl, 5 mM $MgCl_2$, 10 μM $ZnCl_2$ and 0.02% NaN_3 in ^2H_2O. Importantly, there were no significant chemical shift differences for WT or Gly64Ser $3D^{pol}$ between the two buffer systems. For complex formation, the typical final concentrations were 200−250 μM for $3D^{pol}$, 200−500 μM for duplex RNA, 3.1 mM for 3′-dATP, and 4 mM for UTP. In general, a 2:1 duplex RNA:protein ratio was required to saturate $3D^{pol}$

with sym/sub RNA (i.e., for resonances corresponding to the unliganded enzyme to disappear) (see Supporting Information Figure S2). Desalting of the ternary complexes bound with UTP through spin columns did not result in changes to the NMR spectrum, suggesting that this complex is quite stable under NMR conditions.

NMR Spectroscopy. Most NMR experiments were performed on a Bruker Avance III 600 MHz spectrometer equipped with a 5 mm "inverse detection" triple resonance ($^{1}H/^{13}C/^{15}N$) single axis gradient TCI cryoprobe. We also attempted to perform ^{13}C-methyl R_2 relaxation dispersion experiments using a similarly equipped 850 MHz spectrometer. $^{1}H-^{13}C$ HSQC spectra were generally acquired as 64 (t_1) × 512 (t_2) complex matrix, with 64−128 scans per increment and 1.0 s recovery delay. A spectrum for WT 3D^{pol} was also acquired using a recovery delay of 7.0 s but was not qualitatively different (i.e., no new resonances were observed) than spectra acquired with a shorter delay. The spectra of the methionine mutants, along with WT 3D^{pol}, were acquired at 298 K. All other experiments were conducted at 293 K. 4,4-Dimethyl-4-silapentane-1-sulfonic acid (DSS) was used as an external chemical shift reference.

For the metal titrations, $CoCl_2$ was added to protein in varying ratios (1:0.06 to 1:1.7 for protein:metal), and the $^{1}H-^{13}C$ HSQC was recorded. T_1 and T_2 relaxation experiments were performed as described (*39*, *40*). Data for T_1 delays were acquired out to 6.4 s, and data for the T_2 delays were acquired out to 157 ms. T_1 and T_2 experiments were repeated three to four times on two or three separately expressed and purified samples of WT and Gly64Ser 3D^{pol}. R_2 relaxation dispersion experiments were performed according to the pulse schemes in refs *41* and *42* using a total relaxation delay of 10 ms. The R_{ex} values (i.e., R_2 contribution from conformational exchange) were estimated by subtracting the R_2 value estimated under "fast pulsing conditions" (the time between consecutive 180^{o} pulses, $\tau = 500\ \mu s$, $1/\tau = 2000\ s^{-1}$) from the R_2 value estimated under "slow pulsing conditions" ($\tau = 2500\ \mu s$, $1/\tau = 400\ s^{-1}$). All NMR spectra and relaxation data were processed with NMRPipe (*43*) and analyzed with NMRView (*44*).

RESULTS AND DISCUSSION

NMR Assignments of [methyl-^{13}C]Methionine-Labeled 3D^{pol}. We have produced [*methyl*-^{13}C]methionine-labeled 3D^{pol} through overpression of PV 3D^{pol} in a methionine auxotrophic strain of *E. coli* by adapting procedures from previously established protocols (*34*, *36*, *37*). Importantly, we are able to obtain 0.2−0.4 mM protein samples suitable for NMR. Dynamic light scattering measurements indicated that the protein exists as a monomer under the NMR solution conditions (data not shown).

There are 17 methionines scattered throughout the structure of 3D^{pol}, including methionines in the fingers, palm, and thumb subdomains of 3D^{pol} (Figure 1A; see also Supporting Information Table S1). It should be noted that the overexpression and purification procedure yields 3D^{pol} with the correct amino acid (i.e., glycine) at position 1 rather than a methionine (*36*). It has been previously observed that mutations at the amino terminus result in enzymes with altered enzyme kinetics, due in part to structural perturbations to Asp238 that is responsible for properly positioning the incoming nucleotide (*36*, *45*). To assign the resonances in the $^{1}H-^{13}C$ HSQC spectrum of [*methyl*-^{13}C]methionine-labeled 3D^{pol} (Figure 2), we generated mutants in which each methionine residue was substituted with an isoleucine residue (or leucine in the case of Met123Leu). Most of the site mutants resulted in the elimination of a single resonance, allowing for straightforward assignment of all 15 resonances observed for the WT spectrum (Figure 2A). Met286Ile and Met299Ile mutations did not result in the elimination of any resonances, although they did result in some chemical shift changes (Supporting Information Table S2). Both methionine residues belong to motif B and are in close structural vicinity to each other. Mutation of the other methionines did not reveal any other peaks that might be obscured in the WT spectrum. This suggests that the peak intensities for Met286 and Met299 are quite low compared to the other methionines. It should also be noted that binding of RNA and/or nucleotide did not result in any new resonances that might be ascribed to Met286 or Met299.

Paramagnetic Shifts Resulting from Addition of Co^{2+}. We also recorded the $^{1}H-^{13}C$ HSQC of [*methyl*-^{13}C]methionine-labeled 3D^{pol} upon addition of stoichiometric amounts of $MgCl_2$ and $CoCl_2$. It has been previously observed that 3D^{pol} can use Co^{2+} cofactor for catalysis (*35*). Addition of Mg^{2+} had little effect on the 3D^{pol} spectrum, other than a small chemical shift change to Met6 (data not shown), but addition of the paramagnetic ion Co^{2+} resulted in chemical shift changes for Met225, Met323, Met392, and Met394, with smaller chemical shift changes for Met74 and Met354 (Figure 2B). These findings are consistent with the resonance assignments of the methionines. Met225, Met323, and Met354 are all located in the palm region of 3D^{pol} (Supporting Information Table S1) and are relatively near the metal binding sites (12−16 Å) compared to most of the other methionines (> 25 Å). Met392 is also relatively close to the metal binding site, although the orientation of Met394 results in its ε-methyl group being ∼20−21 Å from the metal binding sites. Movement of Met394 or structural changes within the thumb domain may bring Met394 into closer proximity to the metal binding sites. Unfortunately, direct comparison between methionines is problematic considering that the pseudocontact shift resulting from the paramagnetic ion has an angular dependence (*46*, *47*), which is different for each of the effected methionines.

Solvent Accessibility of the Methionines. We also compared the solvent accessibility of the ε-methyl groups of the methionines to the peak intensities (Figure 2D). The peak intensity generally correlated with the solvent accessibility of the methyl probe, as has been previously observed in the DNA damage recognition protein UvrB (*48*). This makes intuitive sense considering that more solvent exposed residues should be less motionally restricted, leading to longer transverse relaxation times (T_2) and more intense peaks (*48*). Of course, one major caveat to this analysis is that exchange broadening can significantly reduce the peak intensities. The Met6 resonance has a much lower signal intensity than what would be expected, suggesting that Met6 might be experiencing exchange broadening, which is consistent with our R_2 relaxation dispersion experiments (see below). The more solvent exposed methionines, Met86, Met123, Met189, Met251, and Met392, also have chemical shifts closer to that of free methionine.

Mutational Analysis of 3D^{pol}. Although the assignment of the [*methyl*-^{13}C]methionine spectrum of PV 3D^{pol} was relatively straightforward using the methionine mutants, some of the methionine mutants led to additional spectral changes (Figure 2C, Supporting Information Tables S2−S4). Some of these spectral changes could be readily rationalized because these

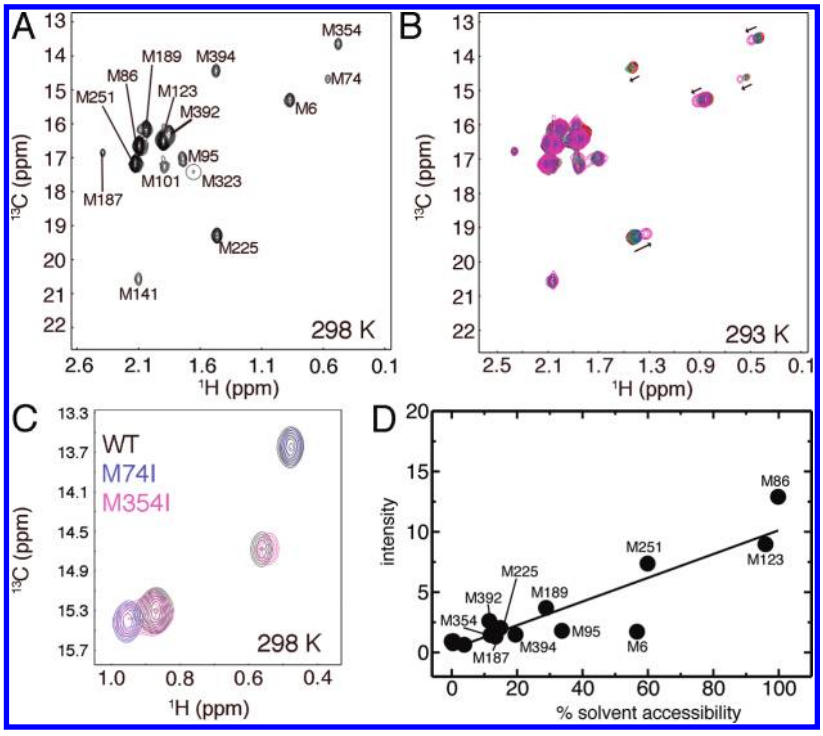

FIGURE 2: Assignment of the [*methyl*-^{13}C]methionine WT 3D^{pol} NMR spectrum. (A) The ^{1}H−^{13}C HSQC spectra of WT 3D^{pol} obtained at 298 K (300 μM 3D^{pol} in 25 mM potassium phosphate, pH 8.0, 150 mM NaCl, 1 mM DTT, 0.02% (w/v) NaN_3 in $^{2}H_2O$). (B) WT 3D^{pol} titrated with the paramagnetic metal Co^{2+} at 293 K. The protein concentration of 3D^{pol} was 180 μM. Co^{2+} concentrations were 0 (black), 10 (red), 50 (green), 100 (blue), and 300 (magenta) μM. (C) Comparion of the ^{1}H−^{13}C HSQC spectra of WT (black), Met74Ile (blue), and Met354Ile (magneta) 3D^{pol} at 298 K. (D) Correlation between solvent accessibility and peak intensity. The percent solvent accessibilities were determined using the GETAREA program with the default radius for the water probe (1.4 Å) (*57*).

methionines make direct interactions or they are spatially close. For example, the backbone nitrogen of Met95 hydrogen bonds to the backbone carbonyl oxygen of Met189. The Met95Ile mutation leads to a small chemical shift change to the Met189 resonance (Supporting Information Table S3), and likewise the Met189Ile mutation leads to a small chemical shift change to the Met95 resonance (Supporting Information Table S4). Met225 and Met323 are in van der Waals contact distance. The Met225Ile mutation leads to a chemical shift change to the Met323 resonance, and likewise the Met323Ile mutation leads to a chemical shift change to the Met225 resonance (Supporting Information Table S4).

However, other spectral changes are less readily rationalized. For example, the Met299Ile mutation leads to chemical shift changes to the Met74 and Met354 resonances (Supporting Information Tables S3 and S4), despite Met299 being ~12 and ~17 Å (distances between α-carbons) away from Met74 and Met354, respectively. An even more dramatic example is the Met74Ile mutation that results in a chemical shift change to the Met95 resonance, despite the α-carbons of these amino acids being ~30 Å apart.

Half of the methionine mutants (9 of 17) also show spectral changes to the Met6 and Met187 resonances. The Met74Ile, Met86Ile, and Met95Ile mutants show similar chemical shift changes to Met6 and Met187 (Supporting Information Table S2). Other methionine mutants (i.e., Met141Ile, Met189Ile, Met251Ile, Met323Ile, and Met354Ile) show two resonances for both Met6 and Met187; one set of resonances overlap that of wild-type 3D^{pol}, whereas the other set of resonances overlap that of Met74Ile/Met86Ile/Met95Ile 3D^{pol} (e.g., Figure 2C; also see Supporting Information Table S2). Mutations leading to this behavior are found throughout 3D^{pol}, including amino acid positions in the fingers (i.e., Met74, Met86, Met95, Met141, Met189, and Met251) and palm (i.e., Met323 and Met354) regions of the enzyme. Some of the mutations are near Met187 (e.g., Met95, Met189), but the mutations are all distant (> 25 Å) from Met6. Intriguingly, the methionine mutations result in similar behavior to both the Met6 and Met187 resonances; that is, whenever there is chemical shift change, or the appearance of two resonances for Met6, there is a corresponding change for Met187. Moreover, the peak ratios between the "major" and "minor" resonances of Met6 and Met187 are very similar for all of the mutants that show two sets of resonances for Met6 and Met187 (Supporting Information Table S5). This suggests that Met6 and Met187 are somehow conformationally coupled despite being > 26 Å apart (α-carbon distance).

Analysis of RNA Binding and Ternary Complexes of Wild-Type 3D^{pol}. To gain more insight into the structural changes to 3D^{pol} that accompany RNA binding and formation of the ternary complex with both RNA and incoming nucleotide bound, we titrated 3D^{pol} with the symmetrical primer/template substrate (sym/sub RNA) previously developed to study the kinetic mechanism of PV 3D^{pol} and nucleotide (Figure 3). Our strategy to "capture" the ternary complex involved first adding 3′-dATP to the enzyme/RNA mixture that would become incorporated into the RNA but then would prevent phosphodiester formation with subsequent nucleotide additions ("3-blocked RNA") (Figure 3A). Importantly, there were no significant chemical shift differences between the enzyme bound to the original sym/sub RNA and after 3′-dATP was added for WT 3D^{pol} (Supporting Information Table S6 and Figure S3), but there were significant chemical shift changes after the addition of the second nucleotide, UTP (Figure 3B,C, Supporting Information Table S6), suggesting that we were

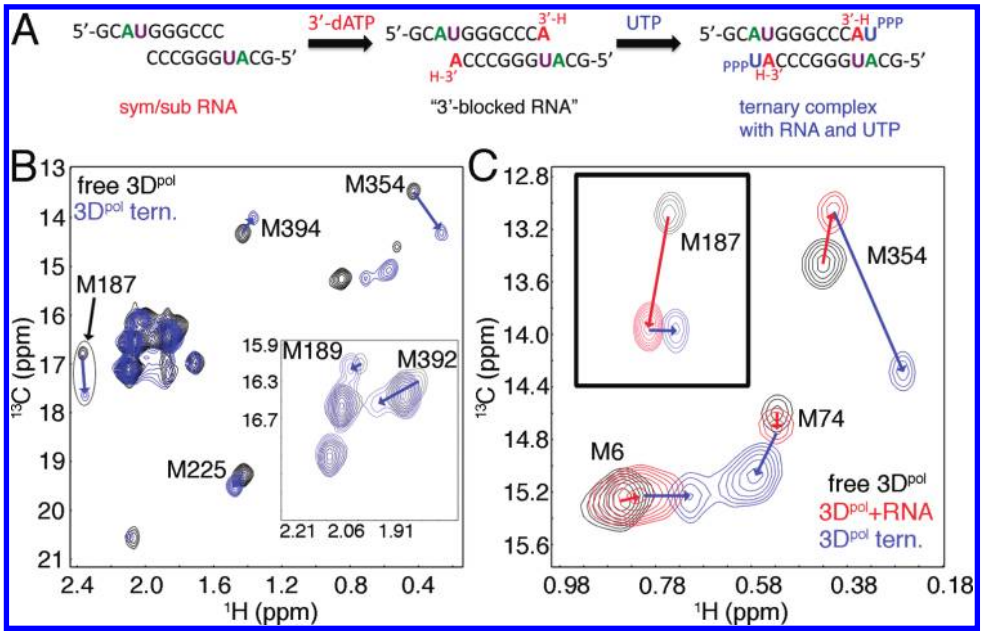

FIGURE 3: Conformational changes upon binding RNA and nucleotide to WT 3D^{pol}. (A) Strategy to generate 3D^{pol} complexes bound with RNA and nucleotide. Addition of 3′-dATP to the 3D^{pol}/RNA reaction mixture will result in nucleotide incorporation into the sym/sub RNA but will prevent additional phosphodiester bond formation with subsequent addition of UTP nucleotide. This will essentially "trap" the enzyme in a ternary complex bound with 3′-blocked RNA and UTP. (B) $^{1}H-^{13}C$ HSQC comparison of WT 3D^{pol} in the unliganded state (black) and in the ternary complex with 3′-blocked RNA and UTP (blue). (C) Close-up of the Met6, Met74, and Met354 resonances showing a comparison between unliganded enzyme (black), enzyme bound with sym/sub RNA (before 3′-dATP addition) (red), and enzyme bound with 3′-blocked RNA and UTP (blue). 3D^{pol} (245 μM) was in $^{2}H_2O$-based 10 mM HEPES, pH 8.0, 200 mM NaCl, 5 mM $MgCl_2$, 10 μM $ZnCl_2$, and 0.02% NaN_3. Sym/sub RNA and UTP were at concentrations of 490 μM (duplex concentration) and 4 mM, respectively. Spectra were acquired at 293 K.

successful in capturing the ternary complex bound with 3′-blocked RNA and UTP.

We observed chemical shift changes when the sym/sub RNA was added and additional chemical shift changes upon formation of the ternary complex, although some methionines showed chemical shift changes only for RNA addition or after ternary complex formation (Supporting Information Table S6). For example, there were chemical shift changes to the Met392 and Met394 resonances when RNA was bound, but there were not any additional chemical shift changes to these resonances once the ternary complex was formed (Supporting Information Table S6). Met392 and Met394 are both on the thumb of the enzyme, and the chemical shift changes may be reporting on the closing of the active site cleft as the fingers and thumbs "wrap" around the RNA. The lack of additional chemical shift changes to these methionine resonances upon formation of the ternary complex with UTP suggests that the conformational change step prior to chemistry is not a global closing of the active site (i.e., any closing of the active site cleft occurs after RNA binding but before ternary complex formation) consistent with previous suggestions for PV 3D^{pol} (*5*). In contrast, the resonance for Met225 only showed a chemical shift change once both RNA and UTP were bound (Supporting Information Table S6). This observation is consistent with rearrangements in motif A (and motif B) that are predicted to occur in order to bring the triphosphate group of the incoming nucleotide into proper alignment for phosphodiester formation.

Other methionines showed chemical shift changes both after RNA and then UTP nucleotide were added (Figure 3). The resonance for Met187 showed a large chemical shift change when RNA was added and then a smaller chemical shift change after forming the ternary complex. Met187 thus appears to be sensitive to RNA binding, which is consistent with crystal structures of FMDV 3D^{pol} that show the equivalent residue to Arg188 in PV 3D^{pol} interacting with RNA (*26*). Smaller changes to this region and/or RNA binding may occur once the ternary complex has formed. Met6 and Met74 also show chemical shifts changes upon RNA binding and formation of the ternary complex. Met6 is on the N-terminal β-strand that makes hydrogen bond interactions with motifs A and B (Figure 1B) and may be reporting indirectly on structural changes in these motifs. Met74 is in the fingers region but makes hydrogen bond interactions with Asp71 and van der Waals contacts with other residues on the $\alpha1-\alpha2$ loop that also interacts with motifs A and B (Figure 1B).

The Met354 resonance has a small chemical shift change when RNA is bound but a much larger chemical shift change upon formation of the ternary complex. Met354 is in motif D that has been suggested to be the most dynamic structural element of 3D^{pol} enzymes (*28*). Motif D has been predicted to undergo a conformational change in order to properly orient the active site acid Lys359 for catalysis (*28*). The large chemical shift change for Met354 upon formation of the ternary complex is consistent with structural rearrangements in motif D.

Solution Structure Comparison between WT and Gly64-Ser 3D^{pol}. We also performed similar RNA and nucleotide binding experiments with Gly64Ser 3D^{pol} (Figure 4). The $^{1}H-^{13}C$ HSQCs of Gly64Ser 3D^{pol} were nearly identical to that of WT 3D^{pol} (Figure 2, Supporting Information Table S6), suggesting that the solution structures of WT and Gly64Ser 3D^{pol} are very similar, consistent with the finding that the crystal structures of the unliganded enzyme are nearly identical (*29*). The only significant chemical shift changes for the unliganded enzymes were for the Met6 and Met74 resonances (Figure 4A). Gly64 makes hydrogen bond interactions with Gly1 on the N-terminal β-strand that includes Met6 (Figure 1B). Upon mutation of Gly64 to Ser,

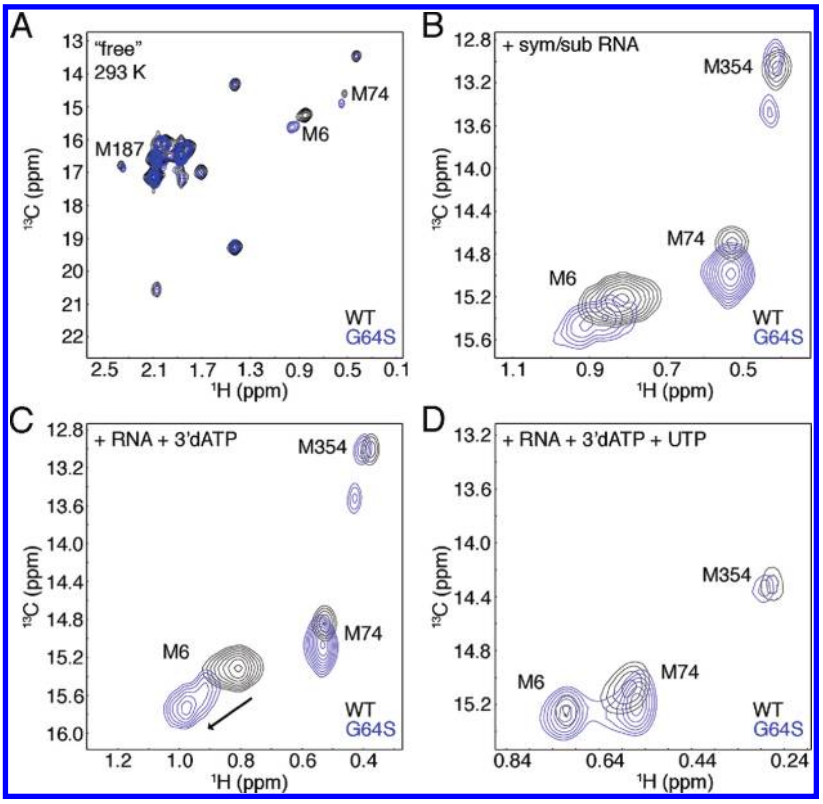

FIGURE 4: Comparison of WT (black) and Gly64Ser (blue) 3D^{pol} in (A) the unliganded form, (B) bound with sym/sub RNA, (C) following reaction with 3′-dATP, and (D) bound with 3′-blocked RNA and UTP. WT (245 μM) and Gly64Ser (200 μM) 3D^{pol} were in $^{2}H_2O$-based 10 mM HEPES, pH 8.0, 200 mM NaCl, 5 mM $MgCl_2$, 10 μM $ZnCl_2$, and 0.02% NaN_3. Sym/sub RNA concentrations for WT (Gly64Ser) 3D^{pol} were 490 (200) μM (B, C) or 490 (400) μM (D). 3′-dATP and UTP concentrations were 3.1 and 4 mM, respectively. Spectra were acquired at 293 K.

there are additional hydrogen bond interactions with the side-chain hydroxyl of Ser64 and the carboxylate group of Glu2 (*29*). This may result in a small conformational change that can be transmited to Met6 through the β-strand, resulting in the observed chemical shift change. However, it should be noted that the N-terminal β-strands of WT and Gly64Ser 3D^{pol} essentially overlap in the crystal structures (rmsd = 0.45 Å for C_α), and the orientation of the side chain for Met6 is identical between WT and Gly64Ser 3D^{pol}. This suggests that the structural and/or dynamic changes for Met6 may only be apparent in solution. Likewise, as previously stated, Met74 is in contact with the $\alpha1-\alpha2$ loop containing Gly64. Mutation to Ser64 may result in structural and/or dynamic changes to the $\alpha1-\alpha2$ loop that results in chemical shift changes to Met74.

Similar chemical shift differences in Met6 and Met74 were observed when RNA was added (Figure 4B). However, there was an additional chemical shift change to Met6 for Gly64Ser 3D^{pol} once 3′-dATP was added that was not observed for the WT enzyme (Figure 4C). Upon addition of UTP, the Met6 resonance then shifted such that it was essentially identical to that of the WT peak position, and there were only minor chemical shift differences for the Met74 and Met354 resonances (Figure 4D, Supporting Information Table S6). This suggests that there are no substantial structural differences between WT and Gly64Ser 3D^{pol} when bound to RNA and UTP in the ternary complex, at least assessed by the conformations and chemical environments of the methionine probes.

It should be noted that when 3′-dATP is added to the reaction mixture, it is in far excess (~3 mM) compared to protein or RNA (~0.2−0.4 mM). Thus, even after the enzyme catalyzes the chemical reaction to form 3′-blocked RNA, 3′-dATP is still in excess and could potentially bind to the protein−RNA complex as an "incorrect" nucleotide. The $^{1}H-^{13}C$ HSQC analysis suggests that WT and Gly64Ser 3D^{pol} form nearly identical ternary complexes when bound with correct nucleotide (i.e., in this case, UTP) (Figure 4D) consistent with their nearly identical rates of phosphodiester formation (*6*), but their ternary complexes with incorrect nucleotide (i.e., with 3′-dATP) are more dissimilar (Figure 4C), at least for the N-terminal β-strand.

Dynamic Comparison between the Apoenzymes of WT and Gly64Ser 3D^{pol}. As has been suggested before, the functional differences between WT and Gly64Ser 3D^{pol} may also be related to the differences in the internal motions of the polymerases (*29*, *30*). NMR provides atomic detail of protein motion over a broad range of time scales (picoseconds to milliseconds) (*49*). For example, the longitudinal (R_1) and transverse (R_2) relaxation rates, along with the heteronuclear nuclear Overhauser effect (heteronuclear NOE), have been used in Lipari−Szabo model-free analysis (*50*, *51*) to yield order parameters (S^2) on the picosecond to nanosecond time scale. Unfortunately, model-free analysis of methyl dynamics using this strategy, especially CH_3 (i.e., no deuterium), is not nearly as robust as that for ^{15}N backbone dynamics (*52*). Moreover, our heteronuclear NOE results were insufficient for quantitative analysis. Instead, we focused on a qualitative comparison between WT and Gly64Ser 3D^{pol} to gauge any differences in their internal protein dynamics that may be related to their functional differences (Figure 5).

We observed significant differences between unliganded WT and Gly64Ser 3D^{pol} in the transverse (T_2) relaxation times for Met6, Met95, Met354, and Met392 (Figure 4). As noted, the N-terminal β-strand containing Met6 interacts with Gly64, and

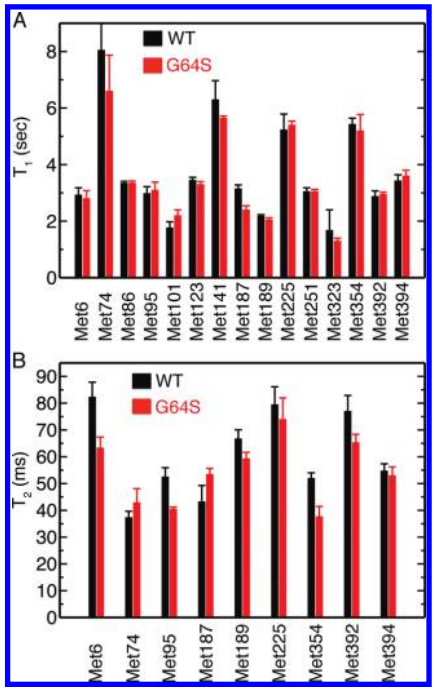

FIGURE 5: Comparion of (A) T_1 and (B) T_2 methyl $^{13}CH_3$ relaxation times for WT (black) and Gly64Ser (red) [*methyl*-^{13}C]methionine-labeled PV 3D^{pol} at 293 K. Protein (250 μM) was in ^2H_2O-based 25 mM potassium phosphate, pH 8.0, 150 mM NaCl, 1 mM DTT, and 0.02% (w/v) NaN_3. The error bars correspond to standard deviations taken from three to four separate experiments.

thus, it is reasonable that mutation of Gly64 could result in changes to the structure and/or dynamics of Met6 and its β-strand. The remaining methionines are more distant from the site of mutation than Met6. The methionines that show differences in T_2 values include residues in the fingers (Met6, Met95), palm (Met354), and thumb (Met392) domains (Supporting Information Table S1), suggesting that the effects of the Gly64Ser mutation are not localized to a single region of the protein.

We did not compare the T_2 values for Met86, Met123, and Met251; these ε-methyl groups are fully solvent exposed, consistent with their T_2 values being much larger (> 190 ms) than the other methionines. We were also unable to compare the T_2 values for Met101, Met141, and Met323; these resonances are too broadened for reliable intensity measurements.

We also attempted to measure the R_2 contribution from conformational exchange (R_{ex}) on the microsecond to millisecond time scale by employing ^{13}C-methyl R_2 relaxation dispersion experiments (*41*, *42*). For the free enzyme, we were only able to observe R_{ex} for Met6, Met187, and Met189. Unfortunately, due to the short T_2 times for the methionines at higher field strength (^{1}H 850 MHz), we were unable to acquire relaxation data at two field strengths that would enable us to quantitatively describe differences in terms of kinetics, thermodynamics, and/or chemical shift differences between exchanging conformations. Nonetheless, we observed significant differences in R_{ex} for Met187 and Met189 between WT (11 s^{-1} for Met187, 7 s^{-1} for Met189) and Gly64Ser 3D^{pol} (27 s^{-1} for Met187, 12 s^{-1} for Met189) by measurement at a single magnetic field strength (^{1}H 600 MHz).

As described with some of the methionine mutants, we observed either chemical shift changes to Met6 and Met187 or two sets of resonances for Met6 and Met187. Together, the results with the methionine mutants and the relaxation data suggest that there is an exchange process involving the conformations of Met6 and Met187, and it is likely that the methionine mutants disturb this conformational equilibrium. Some insight into the conformational equilibrium can be gained by comparing the spectra of methionine mutant 3D^{pol} (e.g., Met251Ile) with wild-type 3D^{pol} in the unliganded and RNA-bound states (Supporting Information Figure S4 and Tables S2 and S6). The second Met187 resonance for Met251Ile 3D^{pol} (and other methionine mutants that show this behavior) is near the Met187 resonance when WT 3D^{pol} is bound to RNA. This suggests that the second conformation for Met187, and the surrounding region, might be involved in the RNA binding mechanism of 3D^{pol}. If the structural differences are assumed to be similar between the exchanging conformations in WT and Gly64Ser 3D^{pol} (i.e., the chemical shift differences between the exchanging conformations are similar), the increased R_{ex} values for Gly64Ser 3D^{pol} may be due to a change in the exchange kinetics or change in the relative populations of the exchanging conformers. Kinetic data comparing the rates of formation of the RNA binding complexes between WT and methionine mutant 3D^{pol} would likely shed more insight into this conformational exchange process and its role (if any) in RNA recognition and/or binding. These studies can also be accompanied with R_2 relaxation dispersion studies with other probes (e.g., Val, Leu, Ile) that might be more amenable to this larger protein system (*32*), as has been performed with the bacteriophage ϕ6 RNA-dependent RNA polymerase (*53*).

Long-Range Interactions in the Function and Fidelity of PV 3D^{pol}. Taken together, our results with Gly64Ser 3D^{pol} and the methionine mutants suggest that there are long-range interaction networks operating throughout PV 3D^{pol} that might be important for its function. One motivation for this study was to gain more insight into the effect of the Gly64Ser mutation on the structure and/or conformational dynamics of 3D^{pol}. Our studies indicate that the Gly64Ser mutation not only affects the conformational environment of those methionines (Met6 and Met74) closest to the site of mutation, but it can have long-range effects on the dynamics of distant amino acid residues. For example, the Gly64Ser mutation can lead to changes to the picosecond to nanosecond time scale dynamics of Met95 and the microsecond to millisecond time scale dynamics of Met187 and Met189, at least in the unliganded enzyme. Close inspection of the 3D^{pol} structure suggests potential path(s) through which changes to Gly64 may affect Met95, Met187, and Met189. Met187 makes van der Waals contact with Ser291 on the highly conserved β10−α13 loop in motif B (Figure 6). The other end of the loop is involved in a hydrogen bond network involving the N-terminal β-strand, Gly64, and motif A (Figure 1B). The β10−α13 loop, including Ser288 and Thr293, is intimately involved in the conformational change that is predicted to reorient the triphosphates of the incoming nucleotide (*19*, *22*, *23*, *26*). A change in the structure and/or dynamics of the loop would help to explain both the effect that Gly64Ser has on the kinetics of the conformational change step and the resulting effect on the dynamics of Met95, Met187, and Met189. A similar conclusion has been recently drawn from crystal structures of FMDV 3D^{pol}. The equivalent Gly64Ser mutation in FMDV 3D^{pol} (Gly62Ser) results in a structural change to the motif B loop resulting in significant changes to the RNA binding mode (*54*). The authors also note extensive hydrogen bond interactions between the α1−α2 loop, the N-terminal β-strand, and motifs A and B that would be able to transmit changes from Gly64 to the active site (*54*). Unfortunately, we were

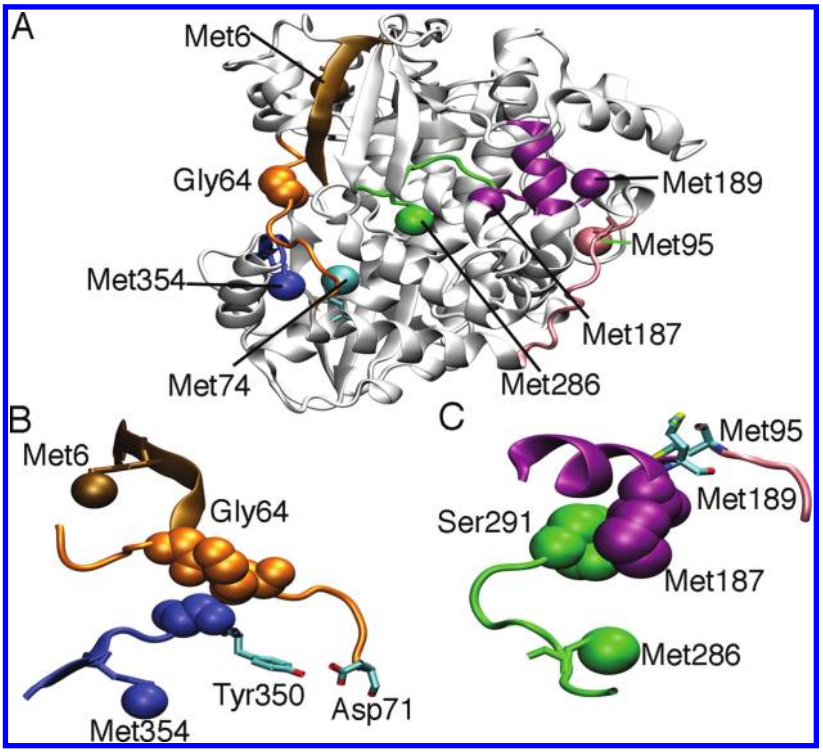

FIGURE 6: Transmission of long-distance signals across the protein structure of PV $3D^{pol}$. (A) Mutation of Gly64 to Ser affects the structure and/or dynamics of distant amino acids, including Met95, Met187, and Met189 on the far side of the protein. (B) The α1−α2 loop (orange) interacts with motif D (blue), including a hydrogen bond interaction between the side chains of Asp71 and Tyr350. (C) Met187 interacts with residues on the β10−α13 loop of motif B, including Ser291. This suggests that Met187 is an indirect probe for the structure/dynamics of the β10−α13 loop. The backbone amide of Met95 hydrogen bonds to the backbone carbonyl of Met189. These interactions, including the hydrogen-bonding network outlined in Figure 1B, allow the transmission of signals from Gly64 all the way to Met95 over 30 Å away.

unable to observe a resonance for Met286 that is on the β10−α13 loop that might have revealed additional information about changes to the structure and/or dynamics of the loop upon mutation of Gly64.

It is intriguing that other mutations in $3D^{pol}$ also caused changes to Met6 and Met187. As stated, although Met6 and Met187 are distant from one another, they appear to be conformationally coupled. Changes to Met6 (or Met187) may be transmitted through a similar network of interactions as suggested for Gly64Ser, considering that Met6 is on the N-terminal β-strand that is involved in the hydrogen-bonding network between motifs A and B and Gly64. Mutations to methionines that are interacting with structural elements containing Met6 or Met187 may induce changes along this long-range network to affect the resonances of both Met6 and Met187. For example, the Met95Ile and Met189Ile mutations induce changes to both Met6 and Met187, likely due to their close interactions with Met187. Likewise, Met141 makes contact with residues (e.g., Leu181, Asn182, Val185) on the α-helix containing Met187. Met323 in motif C interacts with residues in the motif B helix (e.g., Asn301, Asn302, Ile305, Arg306) that can in turn affect the motif B loop and the Met6/Met187 resonances. Met74 and Met251 make contact with residues in the α1−α2 loop (e.g., Val70), and other residues within the same α-helix as Met251 make contact with residues in the β10−α13 loop. The loop immediately preceding Met354 also makes contact with the α1−α2 loop, including a hydrogen bond interaction between the side chains of residues Asp71 and Tyr350 (Figure 6). The chemical shift changes to Met74 and Met354 induced by the Met299Ile (Met299 being in motif B) mutation may also be explained in terms of this network of interaction.

It should be pointed out that although we can trace these networks of interaction through PV $3D^{pol}$, there may be other interactions more important than the interactions we have identified and/or a more complex set of interactions may be responsible for these long-range responses. Moreover, some long-range interactions still remain difficult to rationalize. For example, the Gly64Ser mutation can lead to small changes to the T_2 relaxation time for Met392 (Figure 5), and the Met392Ile mutation can lead to a small chemical shift change to the Met6 resonance (Supporting Information Table S3), even though Met392 is on the thumb domain of $3D^{pol}$ far from Met6 and Gly64 without an easily traceable, direct path of interaction.

Many of the methionines involved in these long-range interaction networks also show chemical shift changes upon binding RNA or formation of the ternary complex with RNA and nucleotide, including Met6, Met74, Met187, Met189, Met354, and Met392, and/or are in regions known to be important for the function and fidelity of $3D^{pol}$, including regions important for nucleotide (motif B), magnesium (motif C, i.e., Asp328 on the same α-helix as Met323), and RNA (e.g., Arg188, Ser291) binding and catalysis (e.g., motif D). Thus, we propose that these long-distance interactions are functionally important and may help to coordinate ligand binding and enzyme catalysis. Similar interaction networks in $3D^{pol}$ have also been suggested to be important for the regulation of polymerase activity by the viral protein 3CD and the formation of higher order replication machinery within the cell (*55*). Long-range interaction networks may also explain the increased thermal stability of $3D^{pol}$ in the presence of nucleotide (*56*). Recent NMR studies of the bacteriophage φ6 RNA-dependent RNA polymerase (*53*) have revealed long-range interactions operating on the microsecond to

millisecond time scale important for the function of this structurally similar enzyme (*53*).

Structural and/or dynamic changes to this network of interactions may thus affect the function and fidelity of PV $3D^{pol}$. In the case of Gly64Ser $3D^{pol}$, these differences include changes to regions important for RNA binding and recognition (e.g., Met95, Met187, Met189), nucleotide recognition (Met6 insofar as it indirectly reports on structural changes in motifs A and B), and phosphodiester bond formation (Met354 in motif D that also contains the general acid Lys359). It is also intriguing that there are more significant chemical shift differences between WT and Gly64Ser $3D^{pol}$ in the ternary complex when bound to the incorrect nucleotide (i.e., E:RNA:3′-dATP) than the correct nucleotide (E:RNA:UTP). Met6 on the N-terminal β-strand especially appears to be responsive to differences between correct versus incorrect ternary complex formation. It was previously observed that mutations to Gly1 result in enzymes with significantly reduced catalytic activity (*36*, *45*), and moreover, these mutations (e.g., Gly1Ala) can significantly affect the interactions with motifs A and B and, in particular, change the orientation of Asp238 (*45*) that is responsible for making hydrogen bond interactions with the incoming nucleotide to properly position the nucleotide for phosphodiester bond formation (*19*−*21*, *45*). Thus, Met6 may be an indirect reporter on the structural changes in motif A. Our findings suggest that there is a conformational change when incorrect nucleotide binds to Gly64Ser $3D^{pol}$ that does not occur when incorrect nucleotide binds to WT $3D^{pol}$, and this difference can be traced to the N-terminal β-strand and, likely, motif A. For Gly64Ser $3D^{pol}$, this may result in a decrease to the conversion rate between "inactive" conformation and catalytically competent conformation when incorrect nucleotide binds compared to what occurs with WT $3D^{pol}$, resulting in a higher fidelity polymerase. NMR studies with other probes (e.g., Val, Leu, Ile) may reveal additional structural and/or dynamic differences between WT and Gly64Ser $3D^{pol}$ and further highlight the roles of the long-range interaction network in the function and fidelity of $3D^{pol}$.

ACKNOWLEDGMENT

We thank Drs. Craig E. Cameron, Ibrahim Moustafa, and Eric Smidansky for insight into polymerase function and fidelity and for critical reading of the manuscript. We also thank Drs. Alan Benesi and Bernie O'Hare for expertise in the collection of the NMR data and members of the Boehr laboratory for valuable input and support.

SUPPORTING INFORMATION AVAILABLE

Table S1 containing a list of all methionines, their locations on the $3D^{pol}$ structure, and primers designed to generate single-site methionine mutants; Tables S2−S4 containing chemical shift data for WT and methionine mutant $3D^{pol}$; Table S5 containing a list of relative peak intensities for the Met6 and Met187 resonances for various methionine mutant $3D^{pol}$; Table S6 containing chemical shift data for WT and Gly64Ser $3D^{pol}$ bound to RNA and nucleotide; Figure S1 comparing $3D^{pol}$ activity under various buffer conditions; Figure S2 containing titration data to determine the optimal ratio of protein and RNA to get fully complexed $3D^{pol}$; Figure S3 comparing WT and Gly64Ser $3D^{pol}$ spectra with different RNA and nucleotide additions; Figure S4 comparing the NMR spectra of unliganded Met251Ile $3D^{pol}$ to WT $3D^{pol}$ in the unliganded state and in the ternary complex. This material is available free of charge via the Internet at http://pubs.acs.org.

REFERENCES

1. Hayden, F. G. (1999) Update on influenza and rhinovirus infections. *Adv. Exp. Med. Biol. 458*, 55–67.
2. Kim, W. R. (2002) The burden of hepatitis C in the United States. *Hepatology 36*, S30–S34.
3. Weiss, S. R., and Navas-Martin, S. (2005) Coronavirus pathogenesis and the emerging pathogen severe acute respiratory syndrome coronavirus. *Microbiol. Mol. Biol. Rev. 69*, 635–664.
4. Hayden, F. G. (2006) Respiratory viral threats. *Curr. Opin. Infect. Dis. 19*, 169–178.
5. Castro, C., Arnold, J. J., and Cameron, C. E. (2005) Incorporation fidelity of the viral RNA-dependent RNA polymerase: a kinetic, thermodynamic and structural perspective. *Virus Res. 107*, 141–149.
6. Arnold, J. J., Vignuzzi, M., Stone, J. K., Andino, R., and Cameron, C. E. (2005) Remote site control of an active site fidelity checkpoint in a viral RNA-dependent RNA polymerase. *J. Biol. Chem. 280*, 25706–25716.
7. Vignuzzi, M., Stone, J. K., Arnold, J. J., Cameron, C. E., and Andino, R. (2006) Quasispecies diversity determines pathogenesis through cooperative interactions in a viral population. *Nature 439*, 344–348.
8. Pfeiffer, J. K., and Kirkegaard, K. (2003) A single mutation in poliovirus RNA-dependent RNA polymerase confers resistance to mutagenic nucleotide analogs via increased fidelity. *Proc. Natl. Acad. Sci. U.S.A. 100*, 7289–7294.
9. Pfeiffer, J. K., and Kirkegaard, K. (2005) Increased fidelity reduces poliovirus fitness and virulence under selective pressure in mice. *PLoS Pathog. 1*, e11.
10. Harki, D. A., Graci, J. D., Galarraga, J. E., Chain, W. J., Cameron, C. E., and Peterson, B. R. (2006) Synthesis and antiviral activity of 5-substituted cytidine analogues: identification of a potent inhibitor of viral RNA-dependent RNA polymerases. *J. Med. Chem. 49*, 6166–6169.
11. Harki, D. A., Graci, J. D., Korneeva, V. S., Ghosh, S. K., Hong, Z., Cameron, C. E., and Peterson, B. R. (2002) Synthesis and antiviral evaluation of a mutagenic and non-hydrogen bonding ribonucleoside analogue: 1-beta-D-ribofuranosyl-3-nitropyrrole. *Biochemistry 41*, 9026–9033.
12. Collett, M. S., Neyts, J., and Modlin, J. F. (2008) A case for developing antiviral drugs against polio. *Antiviral Res. 79*, 179–187.
13. Crotty, S., Maag, D., Arnold, J. J., Zhong, W., Lau, J. Y., Hong, Z., Andino, R., and Cameron, C. E. (2000) The broad-spectrum antiviral ribonucleoside ribavirin is an RNA virus mutagen. *Nat. Med. 6*, 1375–1379.
14. Vignuzzi, M., Wendt, E., and Andino, R. (2008) Engineering attenuated virus vaccines by controlling replication fidelity. *Nat. Med. 14*, 154–161.
15. Ng, K. K., Arnold, J. J., and Cameron, C. E. (2008) Structure-function relationships among RNA-dependent RNA polymerases. *Curr. Top. Microbiol. Immunol. 320*, 137–156.
16. Joyce, C. M., and Benkovic, S. J. (2004) DNA polymerase fidelity: kinetics, structure, and checkpoints. *Biochemistry 43*, 14317–14324.
17. Beard, W. A., and Wilson, S. H. (2003) Structural insights into the origins of DNA polymerase fidelity. *Structure 11*, 489–496.
18. O'Reilly, E. K., and Kao, C. C. (1998) Analysis of RNA-dependent RNA polymerase structure and function as guided by known polymerase structures and computer predictions of secondary structure. *Virology 252*, 287–303.
19. Gohara, D. W., Arnold, J. J., and Cameron, C. E. (2004) Poliovirus RNA-dependent RNA polymerase (3Dpol): kinetic, thermodynamic, and structural analysis of ribonucleotide selection. *Biochemistry 43*, 5149–5158.
20. Gohara, D. W., Crotty, S., Arnold, J. J., Yoder, J. D., Andino, R., and Cameron, C. E. (2000) Poliovirus RNA-dependent RNA polymerase (3Dpol): structural, biochemical, and biological analysis of conserved structural motifs A and B. *J. Biol. Chem. 275*, 25523–25532.
21. Korneeva, V. S., and Cameron, C. E. (2007) Structure-function relationships of the viral RNA-dependent RNA polymerase: fidelity, replication speed, and initiation mechanism determined by a residue in the ribose-binding pocket. *J. Biol. Chem. 282*, 16135–16145.
22. Arnold, J. J., and Cameron, C. E. (2004) Poliovirus RNA-dependent RNA polymerase (3Dpol): pre-steady-state kinetic analysis of ribonucleotide incorporation in the presence of Mg^{2+}. *Biochemistry 43*, 5126–5137.

23. Arnold, J. J., Gohara, D. W., and Cameron, C. E. (2004) Poliovirus RNA-dependent RNA polymerase (3Dpol): pre-steady-state kinetic analysis of ribonucleotide incorporation in the presence of Mn^{2+}. *Biochemistry 43*, 5138–5148.
24. Berdis, A. J. (2009) Mechanisms of DNA polymerases. *Chem. Rev. 109*, 2862–2879.
25. Showalter, A. K., and Tsai, M. D. (2002) A reexamination of the nucleotide incorporation fidelity of DNA polymerases. *Biochemistry 41*, 10571–10576.
26. Ferrer-Orta, C., Arias, A., Perez-Luque, R., Escarmis, C., Domingo, E., and Verdaguer, N. (2007) Sequential structures provide insights into the fidelity of RNA replication. *Proc. Natl. Acad. Sci. U.S.A. 104*, 9463–9468.
27. Castro, C., Smidansky, E., Maksimchuk, K. R., Arnold, J. J., Korneeva, V. S., Gotte, M., Konigsberg, W., and Cameron, C. E. (2007) Two proton transfers in the transition state for nucleotidyl transfer catalyzed by RNA- and DNA-dependent RNA and DNA polymerases. *Proc. Natl. Acad. Sci. U.S.A. 104*, 4267–4272.
28. Castro, C., Smidansky, E. D., Arnold, J. J., Maksimchuk, K. R., Moustafa, I., Uchida, A., Gotte, M., Konigsberg, W., and Cameron, C. E. (2009) Nucleic acid polymerases use a general acid for nucleotidyl transfer. *Nat. Struct. Mol. Biol. 16*, 212–218.
29. Marcotte, L. L., Wass, A. B., Gohara, D. W., Pathak, H. B., Arnold, J. J., Filman, D. J., Cameron, C. E., and Hogle, J. M. (2007) Crystal structure of poliovirus 3CD protein: virally encoded protease and precursor to the RNA-dependent RNA polymerase. *J. Virol. 81*, 3583–3596.
30. Cameron, C. E., Moustafa, I. M., and Arnold, J. J. (2009) Dynamics: the missing link between structure and function of the viral RNA-dependent RNA polymerase? *Curr. Opin. Struct. Biol. 19*, 768–774.
31. Sprangers, R., Velyvis, A., and Kay, L. E. (2007) Solution NMR of supramolecular complexes: providing new insights into function. *Nat. Methods 4*, 697–703.
32. Korzhnev, D. M., Kloiber, K., Kanelis, V., Tugarinov, V., and Kay, L. E. (2004) Probing slow dynamics in high molecular weight proteins by methyl-TROSY NMR spectroscopy: application to a 723-residue enzyme. *J. Am. Chem. Soc. 126*, 3964–3973.
33. Tugarinov, V., and Kay, L. E. (2004) An isotope labeling strategy for methyl TROSY spectroscopy. *J. Biomol. NMR 28*, 165–172.
34. Arnold, J. J., Bernal, A., Uche, U., Sterner, D. E., Butt, T. R., Cameron, C. E., and Mattern, M. R. (2006) Small ubiquitin-like modifying protein isopeptidase assay based on poliovirus RNA polymerase activity. *Anal. Biochem. 350*, 214–221.
35. Arnold, J. J., Ghosh, S. K., and Cameron, C. E. (1999) Poliovirus RNA-dependent RNA polymerase (3D(pol)). Divalent cation modulation of primer, template, and nucleotide selection. *J. Biol. Chem. 274*, 37060–37069.
36. Gohara, D. W., Ha, C. S., Kumar, S., Ghosh, B., Arnold, J. J., Wisniewski, T. J., and Cameron, C. E. (1999) Production of "authentic" poliovirus RNA-dependent RNA polymerase (3D(pol)) by ubiquitin-protease-mediated cleavage in *Escherichia coli*. *Protein Expression Purif. 17*, 128–138.
37. Studier, F. W. (2005) Protein production by auto-induction in high density shaking cultures. *Protein Expression Purif. 41*, 207–234.
38. Arnold, J. J., and Cameron, C. E. (2000) Poliovirus RNA-dependent RNA polymerase (3D(pol)). Assembly of stable, elongation-competent complexes by using a symmetrical primer-template substrate (sym/sub). *J. Biol. Chem. 275*, 5329–5336.
39. Yamazaki, T., Muhandiram, R., and Kay, L. E. (1994) NMR Experiments for the measurement of carbon relaxation properties in highly enriched, uniformly ^{13}C,^{15}N-labeled proteins: Application to ^{13}C alpha carbons. *J. Am. Chem. Soc. 116*, 8266–8278.
40. Farrow, N. A., Muhandiram, R., Singer, A. U., Pascal, S. M., Kay, C. M., Gish, G., Shoelson, S. E., Pawson, T., Forman-Kay, J. D., and Kay, L. E. (1994) Backbone dynamics of a free and phosphopeptide-complexed Src homology 2 domain studied by ^{15}N NMR relaxation. *Biochemistry 33*, 5984–6003.
41. Skrynnikov, N. R., Mulder, F. A., Hon, B., Dahlquist, F. W., and Kay, L. E. (2001) Probing slow time scale dynamics at methyl-containing side chains in proteins by relaxation dispersion NMR measurements: application to methionine residues in a cavity mutant of T4 lysozyme. *J. Am. Chem. Soc. 123*, 4556–4566.
42. Mulder, F. A., Hon, B., Mittermaier, A., Dahlquist, F. W., and Kay, L. E. (2002) Slow internal dynamics in proteins: application of NMR relaxation dispersion spectroscopy to methyl groups in a cavity mutant of T4 lysozyme. *J. Am. Chem. Soc. 124*, 1443–1451.
43. Delaglio, F., Grzesiek, S., Vuister, G. W., Zhu, G., Pfeifer, J., and Bax, A. (1995) NMRPipe: a multidimensional spectral processing system based on UNIX pipes. *J. Biomol. NMR 6*, 277–293.
44. Johnson, B. A., and Blevins, R. A. (1994) NMR View: A computer program for the visualization and analysis of NMR data. *J. Biomol. NMR 4*, 603–614.
45. Thompson, A. A., and Peersen, O. B. (2004) Structural basis for proteolysis-dependent activation of the poliovirus RNA-dependent RNA polymerase. *EMBO J. 23*, 3462–3471.
46. Bose-Basu, B., DeRose, E. F., Kirby, T. W., Mueller, G. A., Beard, W. A., Wilson, S. H., and London, R. E. (2004) Dynamic characterization of a DNA repair enzyme: NMR studies of [methyl-^{13}C]-methionine-labeled DNA polymerase beta. *Biochemistry 43*, 8911–8922.
47. Emerson, S. D., and La Mar, G. N. (1990) NMR determination of the orientation of the magnetic susceptibility tensor in cyanometmyoglobin: a new probe of steric tilt of bound ligand. *Biochemistry 29*, 1556–1566.
48. DellaVecchia, M. J., Merritt, W. K., Peng, Y., Kirby, T. W., DeRose, E. F., Mueller, G. A., Van Houten, B., and London, R. E. (2007) NMR analysis of [methyl-^{13}C]methionine UvrB from *Bacillus caldotenax* reveals UvrB-domain 4 heterodimer formation in solution. *J. Mol. Biol. 373*, 282–295.
49. Boehr, D. D., Dyson, H. J., and Wright, P. E. (2006) An NMR perspective on enzyme dynamics. *Chem. Rev. 106*, 3055–3079.
50. Lipari, G., and Szabo, A. (1982) Model-free approach to the interpretation of nuclear magnetic resonance relaxation in macromolecules. 1. Theory and range of validity. *J. Am. Chem. Soc. 104*, 4546–4559.
51. Lipari, G., and Szabo, A. (1982) Model-free approach to the interpretation of nuclear magnetic resonance relaxation in macromolecules. 2. Analysis of experimental results. *J. Am. Chem. Soc. 104*, 4559–4570.
52. Choy, W. Y., and Kay, L. E. (2003) Model selection for the interpretation of protein side chain methyl dynamics. *J. Biomol. NMR 25*, 325–333.
53. Ren, Z., Wang, H., and Ghose, R. (2010) Dynamics on multiple timescales in the RNA-directed RNA polymerase from the cystovirus {phi}6. *Nucleic Acids Res. 38*, 5105–5108.
54. Ferrer-Orta, C., Sierra, M., de la Higuera, I., Agudo, R., Arias, A., Perez-Luque, R., Escarmis, C., Domingo, E., and Verdaguer, N. (2010) Structure of foot-and-mouth disease virus mutant polymerases with reduced sensitivity to ribavirin. *J. Virol. 84*, 6188–6199.
55. Boerner, J. E., Lyle, J. M., Daijogo, S., Semler, B. L., Schultz, S. C., Kirkegaard, K., and Richards, O. C. (2005) Allosteric effects of ligands and mutations on poliovirus RNA-dependent RNA polymerase. *J. Virol. 79*, 7803–7811.
56. Thompson, A. A., Albertini, R. A., and Peersen, O. B. (2007) Stabilization of poliovirus polymerase by NTP binding and fingers-thumb interactions. *J. Mol. Biol. 366*, 1459–1474.
57. Fraczkiewicz, R., and Braun, W. (1998) Exact and efficicient analytical calculation of the accessible surface areas and their gradients for macromolecules. *J. Comput. Chem. 19*, 319–333.